Article

Characteristics Analysis of the Multi-Channel Ground-Based Microwave Radiometer Observations during Various Weather Conditions

Meng Liu [1,2], **Yan-An Liu** [1,2,3,*] and **Jiong Shu** [1,2]

1   Key Laboratory of Geographic Information Science, Ministry of Education, East China Normal University, Shanghai 200241, China
2   School of Geographic Sciences, East China Normal University, Shanghai 200241, China
3   Yangtze Delta Estuarine Wetland Ecosystem Observation and Research Station, Ministry of Education & Shanghai Science and Technology Committee, East China Normal University, Shanghai 200241, China
*   Correspondence: yaliu@geo.ecnu.edu.cn

Abstract: Ground-based multi-channel microwave radiometers (MWRs) can continuously detect atmospheric profiles in the tropospheric atmosphere. This makes MWR an ideal tool to supplement radiosonde and satellite observations in monitoring the thermodynamic evolution of the atmosphere and improving numerical weather prediction (NWP) through data assimilation. The analysis of product characteristics of MWR is the basis for applying its data to real-time monitoring and assimilation. In this paper, observations from the latest generation of ground-based multi-channel MWR RPG-HATPRO-G5 installed in Shanghai, China, are compared with the radiosonde observations (RAOB) observed in the same location. The detection performance, characteristics of various channels, and the accuracy of the retrieval profile products of the MWR RPG are comprehensively evaluated during various weather conditions. The results show that the brightness temperatures (BTs) observed by the ground-based MWR RPG during precipitation conditions were high, which affected its detection performance. The bias and the standard deviation (SD) between the BT observed by MWR RPG and the simulated BT during clear and cloudy sky conditions were slight and large, respectively, and the coefficient of determination (R^2) was high and low, respectively. However, when the cloud liquid water (CLW) information was added when simulating BT, the bias and the SD of the observed BT and the simulated BT during cloudy days were reduced and the R^2 value improved, which indicated that CLW information should be taken into account when simulating BT during cloudy conditions. The temperature profiles of the MWR retrieval had the same accuracy of RMSEs (root-mean-square error) with heights during both clear-sky and cloudy sky conditions, where the RMSEs were below 2 K when the heights were below 4 km. In addition, the MWR RPG has the potential ability to retrieve the temperature inversion in the boundary layer, which has important application value for fog and air pollution monitoring.

Keywords: ground-based microwave radiometer; accuracy evaluation; brightness temperature; cloud liquid water; temperature profile; temperature inversion

1. Introduction

High spatial and temporal resolution atmospheric profiles are important for understanding the thermal and dynamical structure of weather processes at various scales [1]. At present, radiosonde observations (RAOB) can provide highly precise vertical atmospheric profiles. However, due to the high observation cost, the low spatial resolution, the distance between weather stations of about 300 km or more, and the low temporal resolution (12 h), radiosonde observations are not sufficient to provide fine variations of vertical atmospheric profiles [2]. Meteorological satellites are affected by the complex surface, resulting in atmospheric profiles near the ground that are not very good. The ground-based microwave

radiometer (MWR) is a new type of detection equipment belonging to passive remote sensing, and mainly measures the downward radiance from the Earth's atmosphere. It can continuously detect temperature and humidity profiles of the atmosphere at 0–10 km altitude near the ground, which is a useful supplement to radiosonde data and satellite data [3]. Meanwhile, ground-based MWRs represent important areas for the development of atmospheric sounding operations, given the great potential of ground-based vertical sounding information in improving small-scale and medium-scale forecast operations [4]. At present, ground-based MWR is mainly dominated by RPG-HATPRO and MP-3000, but ground-based MWR has developed rapidly in China in recent years. The main devices include QFW-6000, MWP967KV, and HT-GMWR. The related profile products are widely used in the fields of artificial weather impact, meteorological protection services for major events, aviation meteorology, urban pollution monitoring, etc.

With the significant increase in the application of multi-channel ground-based MWRs in meteorological operations, it is important to examine the detection performance of this remote sensing equipment. Monitoring the observed brightness temperature (BT) minus the background simulated BT is critical to detect and possibly eliminate any systematic errors in MWR measurements, radiative transfer models, or NWP model predictions [5]. De Angelis et al. [5] and Liu [6] analyzed ground-based MWR BT detection and compared it with simulated BT during clear sky conditions. Ahn et al. [7] compared the simulated BT and the observed BT of MWR during all sky and clear sky conditions. It was found that liquid water in clouds caused a large bias between the observed and the simulated data. It was considered that the cloudy data were not suitable for evaluating the performance of the radiometer, and it was necessary to use the cloudy detection instrument to screen the BT data of the radiometer when there was cloud. However, what has not been considered in the existing research is the effect of adding cloud liquid water (CLW) information to the simulated BT on the observed BT evaluation and the reliability of observed BT during precipitation.

The MWR receives the radiation emitted from the atmosphere in the microwave band of the spectrum and retrieves it into variables such as temperature, relative humidity, and absolute humidity. A lot of research has been conducted on the retrieval methods of ground-based MWRs. The common methods include Bayesian maximum probability estimation algorithm [8], one-dimensional variational retrieval method [9], statistical regression method [10], and neural network method [11]. Li et al. [12] and Li et al. [13] improved the temperature and humidity profiles retrieval during clear-sky and cloudy-sky conditions. Tan et al. [14] established an atmospheric profile retrieval method based on principal component analysis and stepwise regression. It was found that the retrieved profiles captured the evolution of atmospheric conditions very well. Moreover, there are many studies evaluating the accuracy of MWR retrieval profiles. For example, Liu [6] compared the temperature profiles measured by the MWR with sounding temperature profiles. The study explored the effects of altitudes, seasons, and precipitation conditions on the performance of ground-based MWR retrieval temperature profiles. Chan [15] studied the application of ground-based MWR retrieval profiles in strong convective weather. It was found that the radiometer could provide effective information for precipitation forecasting, though there were some differences between ground-based MWR data and RAOB data. Xu et al. [16] compared MWR retrievals and RAOB data during clear-sky and cloudy-sky conditions, and analyzed MWR retrieval accuracies under low, middle, and high clouds identified by IRT. It was found that the accuracy of the retrieval profiles in the lower levels were better than those in the upper levels, and the cloudy profiles were better than those in the clear-sky. Both the temperature profile under high cloud and the vapor density profile under middle cloud had high accuracy. Bedoya-Velásquez et al. [17] used RAOB data to analyze the seasonal periodicity of temperature profiles, relative humidity profiles, and integrated water vapor measured by MWRs. It was found that the biases of the radiometer were small during clear sky and dry conditions, but they were very large during cloudy sky conditions.

MWR soundings are found to be equivalent in accuracy to radiosonde soundings when used for NWP [18]. Several studies using MWR retrieval profiles have shown that they have the potential to improve the forecasting of local weather processes. For example, Olivier et al. [19] used the 3DVAR data assimilation system of Arome-WMed to assimilate the temperature and the humidity profiles of 13 ground-based MWRs. It was found that, in addition to limited improvement in the prediction of large accumulated rainfall, the prediction impact on other upper air and surface meteorological elements was usually neutral. He et al. [20] used WRFDA to assimilate the temperature and humidity profiles of two ground-based MWRs for a heavy rainfall event in Beijing, China. The results showed that the assimilation of ground-based MWR data improved the forecast of precipitation intensity and distribution in the early stage of precipitation, while the assimilation of two ground-based MWRs improved the forecast of a large area heavy precipitation system less as the storm system developed. Qi et al. [21] and Qi et al. [22] used the rapid-refresh multi-scale analysis and prediction system-short term to predict the intensity and distribution of precipitation over a large area using the 3DVAR assimilation technique in the Beijing area. The level-2 products of five ground-based MWRs were assimilated to improve precipitation and echo forecasting, and accurately forecast the band echo splitting and precipitation enhancement process in Beijing. Wave et al. [18] described an example of improving fog prediction based on variational assimilation of radiometric soundings. Temimi et al. [23] evaluated the potential of MWR for nowcasting of fog formation and dissipation in hyper-arid environments by analyzing its profiles.

In this paper, the 2017–2019 observations of HATPRO-G5, the latest generation of RPG ground-based multi-channel MWR installed in Shanghai, China (31.39° N, 121.44° E, 5.5 m above sea level), are compared with the RAOB data to comprehensively evaluate its detection performance, operational stability, and the performance of the temperature retrieval profiles during various weather conditions. The study aims to lay the foundation for the application of this ground-based MWR BT data and temperature profile retrieval product.

The article has been organized in the following way. Section 2 presents the data and methods used in the study, including the ground-based MWR data, data pre-processing process, and the methods of statistical analysis. The analysis of the observed BT characteristics during various weather conditions is described in Section 3. Section 4 discusses the effect of CLW on BT simulations. Section 5 describes the accuracy of temperature retrieval profiles and the performance of temperature inversion retrieval. Finally, Section 6 summarizes the conclusions.

2. Data and Methods

2.1. Data Description

The output data of the new generation of MWR RPG includes level-1 data (BTs) and level-2 data (retrieved products). For level-1 data, seven channels of the RPG humidity profiler were selected with frequencies respectively centered at 22.24, 23.04, 23.84, 25.44, 26.24, 27.84, and 31.40 GHz and seven channels of the RPG temperature profiler were selected with frequencies respectively centered at 51.26, 52.28, 53.86, 54.94, 56.66, 57.30, and 58.00 GHz. For the remote sensing mechanism of the MWR, when it is observed at the zenith, the BT at different heights is related to the molecular density and the temperature of its corresponding layer. Since the spectral center position of any given channel is different, the individual transparency for each channel is, thus, different and the microwave signals reaching the ground reflect the temperature and humidity information at different altitudes [4]. Therefore, MWR can continuously detect the temperature, humidity, and CLW profiles in the atmospheric boundary layer and troposphere in the vertical range of 0–10 km in real time. In this work, the products using MWR RPG level-2 data included atmospheric temperature profile retrieval products, all of which contained 93 altitude layers. In this paper, observations from the latest generation of ground-based multichannel MWR RPG-HATPRO-G5, installed in Shanghai, China, are compared with the RAOB data

observed in the same location. To ensure data quality, liquid nitrogen calibration was carried out once every six months.

2.2. Data Pre-Processing

To evaluate the performance of profile products, the atmospheric temperature profiles of MWR RPG and RAOB data were processed as follows: the time of the two types of temperature profiles was kept consistent; the data of instrument detection anomalies (e.g., the missing RAOB data below 10 km) was eliminated to avoid large errors in interpolation; the two types of temperature profile information were kept highly unified. According to the functional specifications formulated by the China Meteorological Administration to regulate the standards of ground-based MWRs, the vertical height of the atmospheric temperature profiles was uniformly interpolated into 83 layers of the national standard. In addition, the temperature profiles had vertical resolutions of 25 m from the surface to 500 m, 50 m from 500 m to 2000 m, and 250 m from 2000 m to 10,000 m.

In addition, since the BT information detected by the ground-based MWR is the basis for its profile retrieval and assimilation, the quality and the stability of various channels of BT data directly affect the retrieval and assimilation performance. The Monochromatic Radiative Transfer Model (MonoRTM) has been commonly used for BT simulation in microwave bands with high accuracy [7,14]. Its BT simulation requires information on atmospheric temperature, humidity, and liquid water content at different altitudes as input. It can achieve higher accuracy for BT simulation in the presence of cloud coverage. In our work, the temperature and humidity profiles from RAOB and the CLW from ERA5 reanalysis data were used as input data sets for BT simulation calculations, and the same 14 channels of BT as for MWR RPG were taken as outputs for comparison.

This work also classified the BT data and the temperature profiles into "Clear-Sky", "No-precipitating Cloud" and "Precipitating Cloud", according to various weather conditions. Specifically, conditions with precipitation were classified as "Precipitating Cloud", and those without precipitation were classified as "Clear-Sky" or "No-precipitating Cloud", according to the relative humidity. The condition of "Clear-Sky" related to relative humidity of the RAOB being less than 85% in all altitude layers, and that of "No-precipitating Cloud" to relative humidity of one or more layers of the RAOB data being greater than, or equal to, 85%.

2.3. Methods of Statistical Analysis

The characteristics of the MWR RPG observed BT were analyzed by comparing the bias and standard deviation (SD) of the MWR RPG observed BT with the MonoRTM simulated BT. The coefficient of determination (R^2) was used to describe the degree of fit of the observed BT to the simulated BT. Let n be the size of the sample used for comparison. bias, SD, and R^2 are given by:

$$\text{bias} = \frac{1}{n} \sum_{i=1}^{n} (O_i - B_i) \tag{1}$$

$$\text{SD} = \sqrt{\frac{\sum_{i=1}^{n} (X_i - \overline{X})^2}{n}} \tag{2}$$

$$R^2 = \frac{\sum_{i=1}^{n} (\hat{y}_i - \overline{y}_i)^2}{\sum_{i=1}^{n} (y_i - \overline{y}_i)^2} \tag{3}$$

In the above three equations, O_i (with i being the label of the sample) is the MWR RPG observed BT, B_i represents the MonoRTM simulated BT, X_i the calculation of the observed BT minus simulated BT (OMB), $\overline{X}$ means the average value of OMB, y_i stands for the true value of the observed BT, $\overline{y}_i$ denotes the average value of y_i, and $\hat{y}_i$ gives the MWR RPG observed BT predicted by linear fitting equation.

The performance of the temperature profiles retrieved by MWR RPG was evaluated by comparing the bias and RMSE calculated by radiosonde data. Let n be the size of the sample used for comparison. The profile retrieved by MWR RPG was taken as O_i. The profile detected by radiosonde was taken as B_i. The calculation of bias is shown in Equation (1), and the RMSE is given by:

$$\text{RMSE} = \sqrt{\frac{\sum_{i=1}^{n}(O_i - B_i)^2}{n}} \tag{4}$$

3. Brightness Temperature Characteristics Analysis during Various Weather Conditions

First of all, we analyzed the all-sky BT data of MWR RPG observations that included precipitation epochs, followed by analyzing the observed BT of non-precipitation epochs. In addition, when analyzing the observed BT performance of the no-precipitating cloud, the influence of whether or not to add CLW information for BT simulation on the evaluation of BT performance was analyzed.

3.1. Characteristics Analysis of All-Sky Brightness Temperature Data

All successfully matched BT data were compared and analyzed. There were 1749 BTs for each channel, and 335 of them were measured during precipitation conditions. The OMB of 14 channels was plotted over time (Figure 1). The left column of Figure 1 shows the time series plots of OMB for the seven humidity channels and the right column shows the time series plots of OMB for the seven temperature channels. It can be seen that the OMB of the humidity channels was larger than that of the temperature channels, overall. Moreover, we can see that the overall change trend of OMB before and after each MWR calibration was the same, indicating that there was no significant change in the BT detection of each channel before and after the MWR calibration and the detection performance was more stable. Besides, for the all-sky BT data, except for precipitation times, OMB was mostly around zero and precipitation times of the observed BT had a large positive bias. The water vapor channels were mainly used to detect the water vapor information in the atmosphere near the ground. There was water on the waterproof cover of the equipment during precipitation, resulting in a large difference between the observed BT and the simulated BT (without considering the water accumulation). This suggested that the high BT measured by the ground-based MWR RPG during precipitation conditions affected the performance of the observation.

3.2. Characteristics Analysis of Clear-Sky Brightness Temperature Data

For the performance analysis of the BT of MWR RPG observations during non-precipitation conditions, there were 368 BTs for each channel during clear-sky conditions without clouds and the time series of their OMB are shown in Figure 2. It can be seen that the range of OMB for each channel during clear-sky conditions was significantly reduced, as compared with Figure 1, where the ranges of OMB values for various channels showed discrepancies within 10 K. There were obvious positive biases for all humidity channels in the left columns and the 51.26 and the 53.86 GHz temperature channels in the right columns, i.e., the observed values were large. In addition, there was some seasonal variation in the OMB of the near-surface temperature channel during clear-sky conditions. That is, a systematic bias with time dependence was seen with larger values of OMB in winter and spring and smaller values of OMB in summer and autumn. The systematic deviation characteristic was obviously related to the ambient temperature. Since the microwave radiometer required very high thermal stability for the receiver, which should not exceed 0.02 k, it needed a temperature controller to adjust the receiver temperature through heating control. Its working performance in winter and summer should be different to some extent, which might have led to this seasonal variation characteristic. However, the exact cause needs further confirmation.
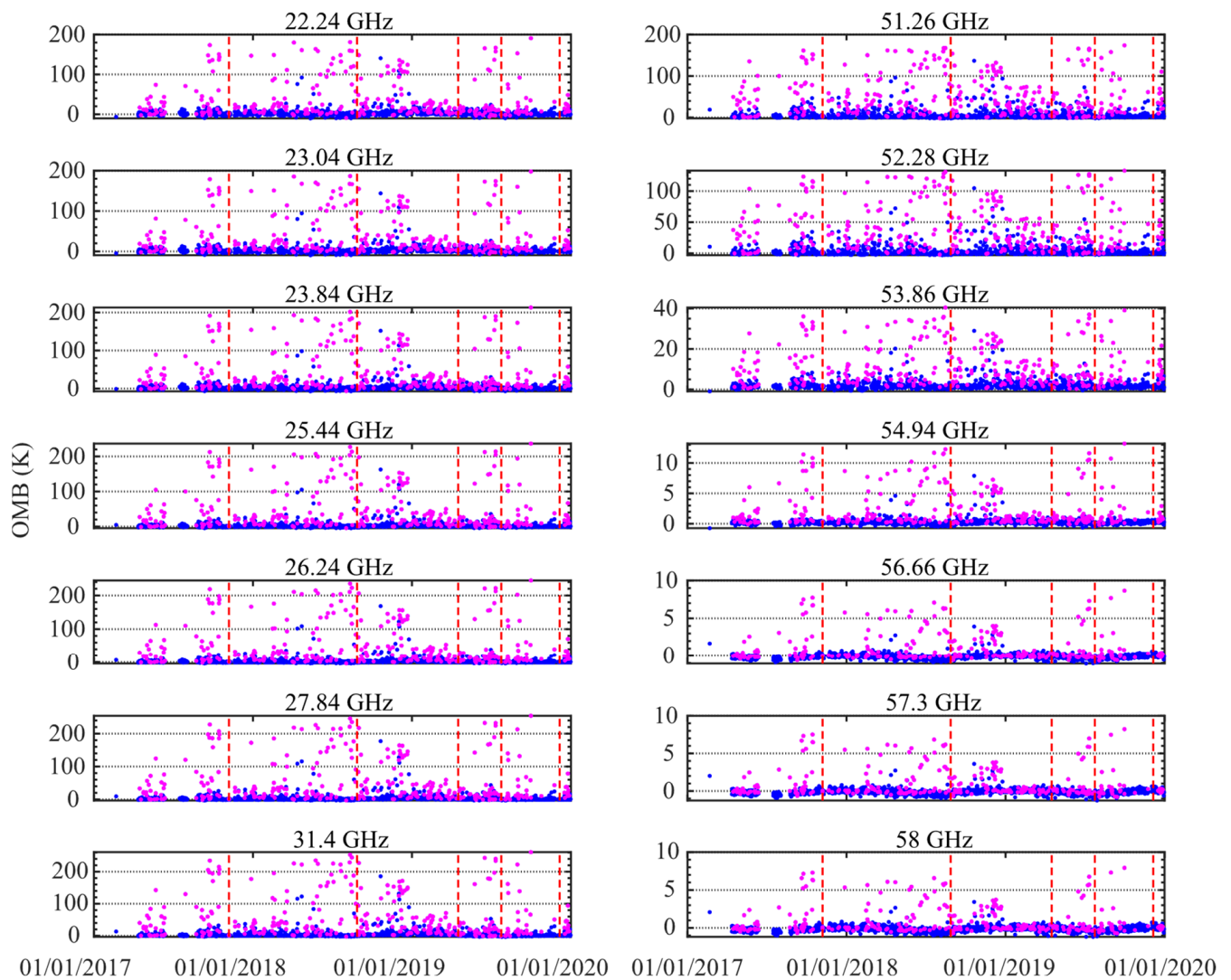
Figure 1. Time series diagrams of OMB of 14 channels, where the pink dots are precipitation times, the blue dots stand for non-precipitation times, and the red dashed lines represent the dates of MWR calibration (7 November 2017, 28 August 2018, 17 April 2019, 25 July 2019, and 6 December 2019).

To further evaluate the difference between the observed BT of MWR RPG and the simulated BT of MonoRTM during clear-sky conditions, the bias, SD, linear fit equation, and R^2 of the observed BTs and the simulated BTs at clear-sky times were calculated, and scatter plots were made for each channel (Figure 3). It can be seen that, except for the 52.28, 56.66, 57.3, and 58 GHz channels, all other channels had small positive biases with the highest bias (1.55 K) located at the 51.26 GHz channel. The bias of each channel showed that there was a systematic bias for further validation. The channel of 22.24–23.84 GHz had a larger SD (>2 K) as compared with the other channels, where the data were more discrete with a larger difference between the observed BT and simulated BT. In addition, the fit coefficients of all channels were high, with the R^2 values above 0.99. Especially for the 54.94–58 GHz channels, the R^2 reached 1, implying that the observed BTs of MWR RPG during clear-sky conditions were in good agreement with the simulated BTs of MonoRTM. It should be noted that the overall fitting coefficients varied somewhat among channels, which was related to the absorption lines of each channel. For the water vapor and oxygen absorption peak regions in the K and V bands, the corresponding detection heights were low and the fitting coefficients were high, especially for the 54.94–58 GHz channel in the V band. However, for the absorption valley area, due to the high detection height, weak

energy signal, and low R^2, the difference and fluctuation of measured and simulated BTs were large. Overall, the observed BT performance of the temperature channels was better than that of the humidity channels in terms of the bias, SD, and R^2 of the observed BTs.
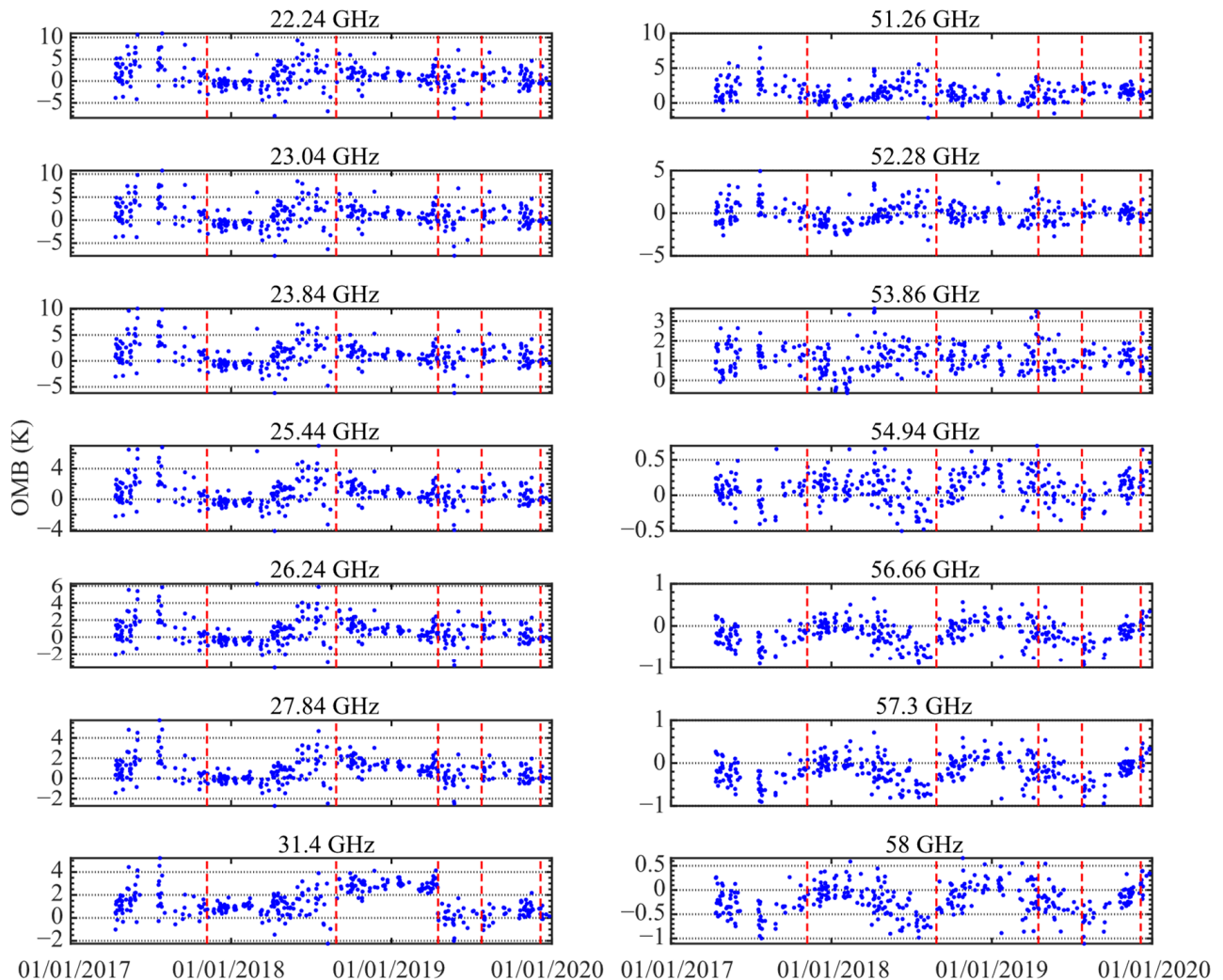

Figure 2. Time series diagrams of OMB of 14 channels in the clear sky (the red dashed lines are the dates of MWR calibration).

3.3. Characteristics Analysis No-Precipitating Cloudy Brightness Temperature Data

For the performance analysis during non-precipitation conditions, there were 1046 BTs for each channel during no-precipitating cloudy conditions. The time series plots of OMB are shown in Figure 4. It can be seen that the range of OMB for each channel during no-precipitating cloudy conditions was significantly smaller as compared with the all-sky BT (Figure 1), but most of the channels had a larger range of OMB as compared with the clear-sky BT (Figure 2). The OMB value ranges of various channels were slightly different. All channels, except for 56.66–58 GHz, had obvious positive biases, and most of their OMB values were concentrated within ±10 K. The OMB values of 56.66–58 GHz channels were concentrated within ±1 K. In addition, consistent with the clear sky, there was some seasonal variation in the OMB of the near-surface temperature sounding channels during cloudy conditions.
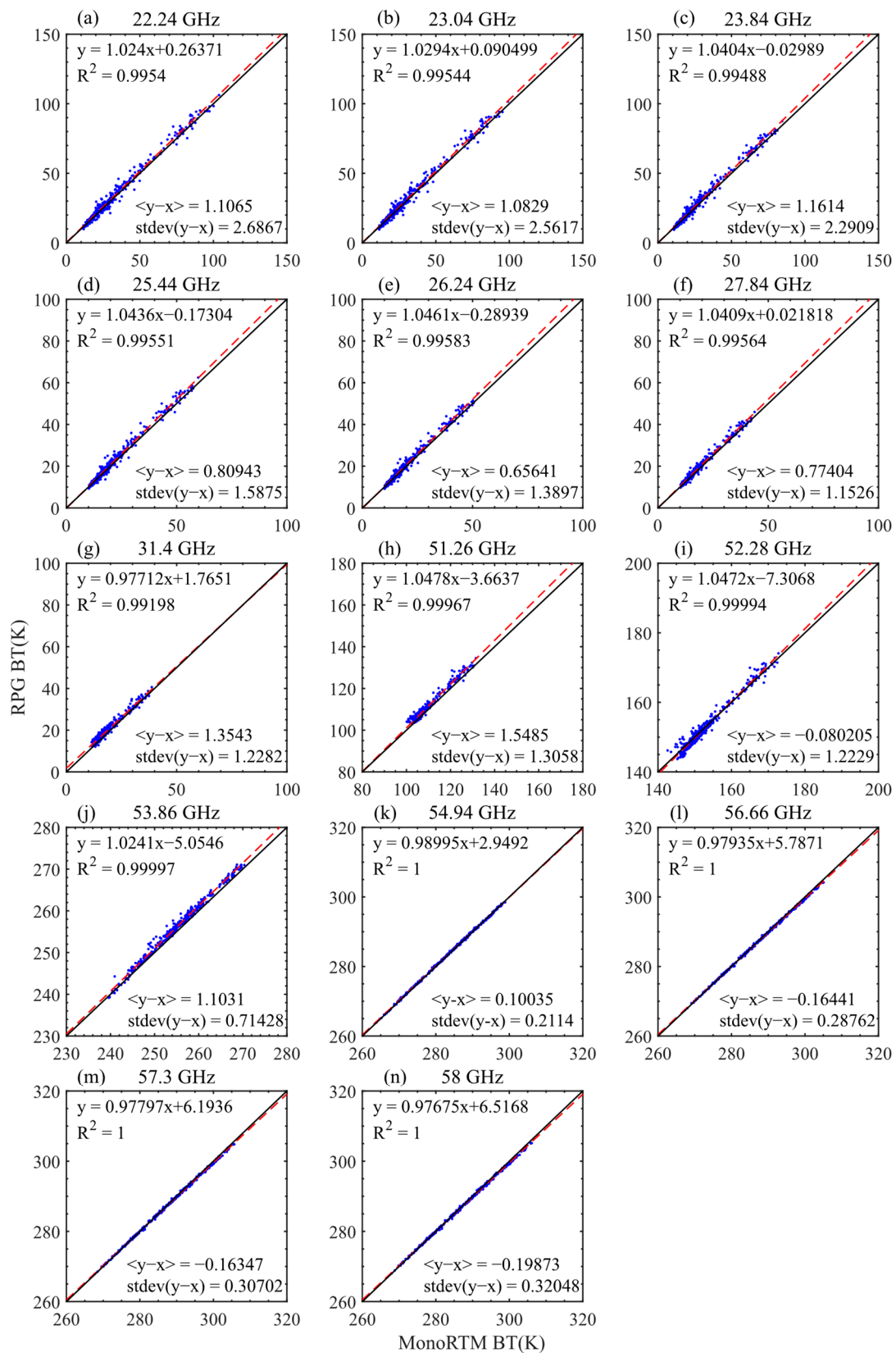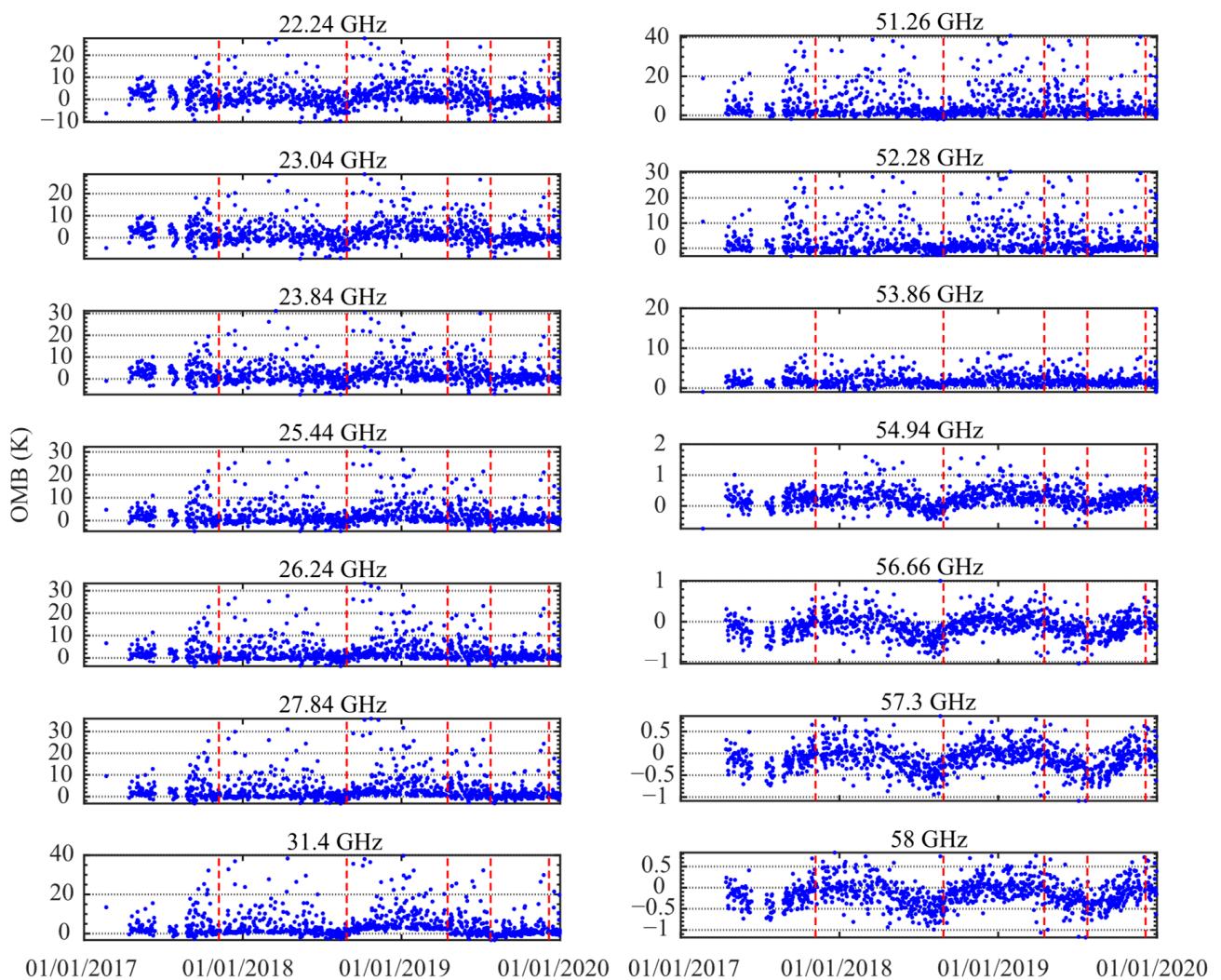
Figure 3. Scatter diagrams of observed BTs and simulated BTs in the clear sky (the red dashed lines denote fitting straight lines). (**a**) 22.24 GHz, (**b**) 23.04 GHz, (**c**) 23.84 GHz, (**d**) 25.44 GHz, (**e**) 26.24 GHz, (**f**) 27.84 GHz, (**g**) 31.40 GHz, (**h**) 51.26 GHz, (**i**) 52.28 GHz, (**j**) 53.86 GHz, (**k**) 54.94 GHz, (**l**) 56.66 GHz, (**m**) 57.30 GHz, and (**n**) 58.00 GHz.

Figure 4. Time series diagrams of OMB of 14 channels in the no-precipitating cloudy weather (the red dashed lines are the dates of MWR calibration).

In order to accurately analyze discrepancies between the observed BT of MWR RPG and the simulated BT of MonoRTM during no-precipitating cloudy conditions, the bias, SD, linear fit equation, and R^2 of the observed BTs and the simulated BTs during cloudy conditions were calculated and scatter plots were made for each channel (Figure 5). It can be seen that, except for the 56.66–58 GHz channels, the scatter distributions of the other channels were more discrete and all of them had positive biases. Furthermore, the bias and SD were larger than the values during clear-sky conditions, where the largest bias and SD occurring at the 51.26 GHz channel were 5.2994 K and 7.3139 K, respectively. In addition, the R^2 values of all channels were above 0.9. Especially, the R^2 values of the 54.94–58 GHz channels reached one. As compared with the clear-sky conditions, the R^2 values of some channels were slightly lower but still remained at a high level. Overall, the systematic bias of the BTs observed by MWR RPG during the no-precipitating cloud was larger and the correlation with the simulated BTs was lower compared with clear-sky.
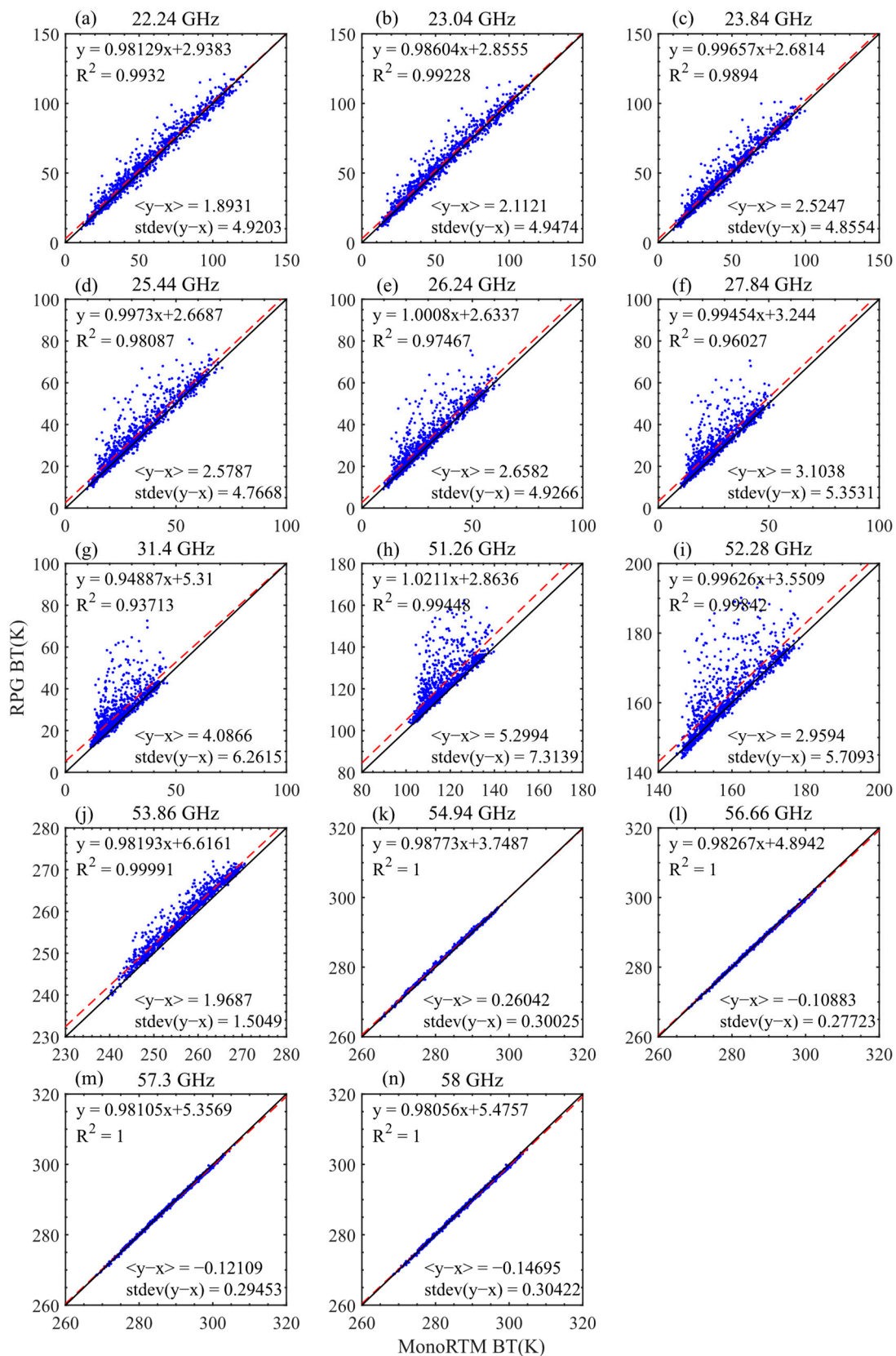
Figure 5. Scatter diagrams of observed BTs and simulated BTs in the no-precipitating cloudy weather (the red dashed lines are fitting straight lines). (**a**) 22.24 GHz, (**b**) 23.04 GHz, (**c**) 23.84 GHz, (**d**) 25.44 GHz, (**e**) 26.24 GHz, (**f**) 27.84 GHz, (**g**) 31.40 GHz, (**h**) 51.26 GHz, (**i**) 52.28 GHz, (**j**) 53.86 GHz, (**k**) 54.94 GHz, (**l**) 56.66 GHz, (**m**) 57.30 GHz, and (**n**) 58.00 GHz.

4. Effect of Cloud Liquid Water on Brightness Temperature Simulation

The radiative transfer model includes a parameterization of CLW absorption that can be selectively used for non-scattering microwave simulations. The implementation of calculating the optical depths based on the input CLW mass mixing ratio follows Turner, Kneifel, and Cadeddu [24]. For the no-precipitating cloudy conditions, since there are large differences between the observed BT of the MWR RPG and the simulated BT of MonoRTM, our work compared these two types of BT with the addition of CLW. Figure 6 shows the sequences of the differences between the observed and simulated BTs (with CLW). Except for the 54.94–58 GHz channel, Figure 6 shows that the positive biases of OMBs decreased, and OMBs with CLW were closer to 0 than OMBs without CLW. It shows that adding liquid water information could significantly reduce the biases caused by cloud influence. In addition, the addition of CLW information could make the seasonal variation of the OMB of the near-surface temperature sounding channels more obvious.
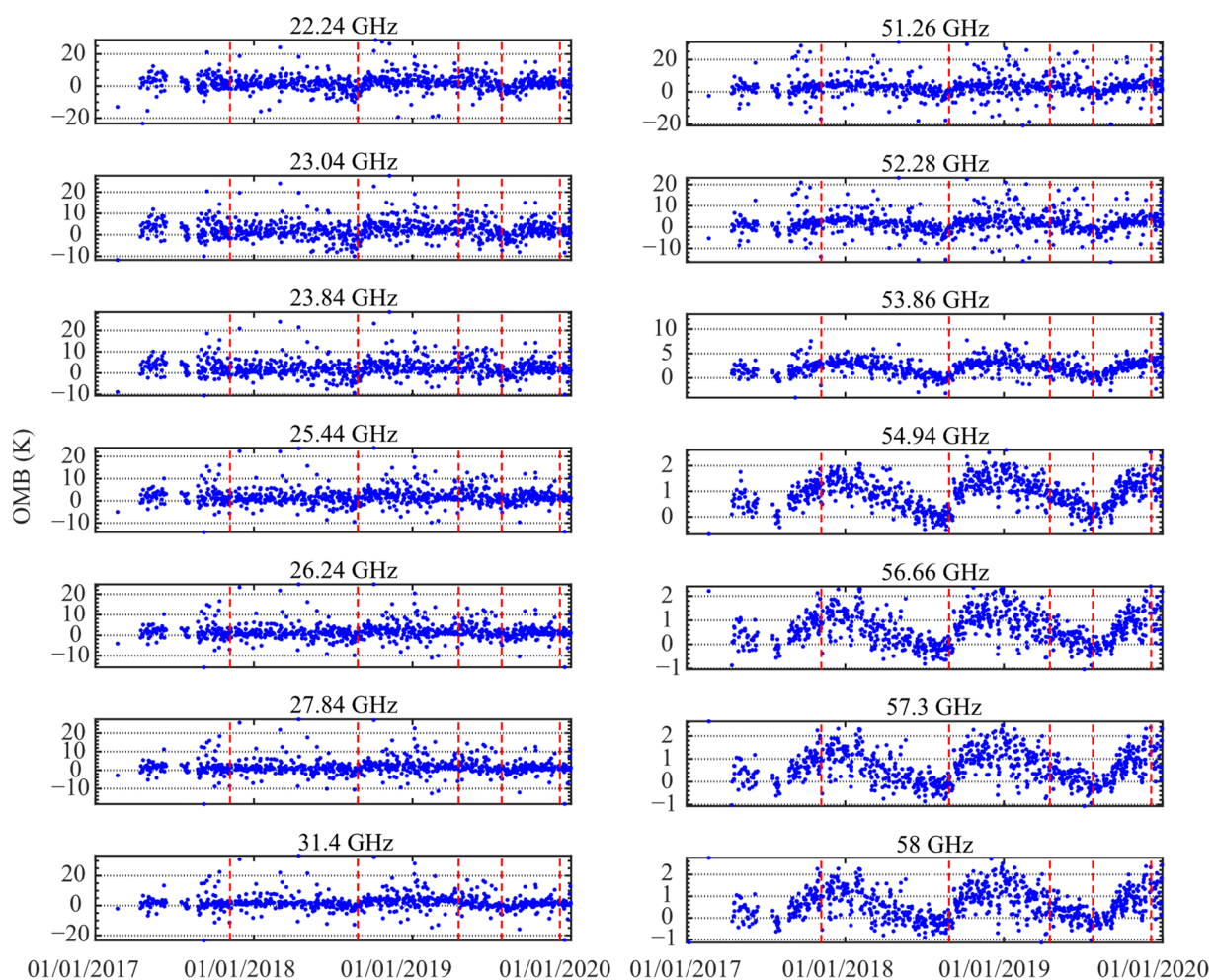
Figure 6. Time series diagrams of OMB (with CLW) of 14 channels in the no-precipitating cloudy weather (the red dashed lines are the dates of MWR calibration).

In the presence of clouds, to accurately tell the differences between the observed BT of MWR RPG and the simulated BT with the addition of CLW information, the bias, SD, linear fit equation, and R^2 between the observed and the simulated BTs were calculated, and scatter plots were made for each channel (Figure 7). By comparing Figure 7 with Figure 5, both bias and SD for the 25.44–52.28 GHz channel were reduced after adding CLW information, the systematic bias was reduced, and the dispersion was weakened as well. The largest bias and SD at the 51.26 GHz channel were 3.2023 K and 5.8595 K, respectively.

For both the 31.4 GHz and 51.26 GHz channels, the biases of the observed BT and the simulated BT were reduced by about 2 K and their SDs were reduced by more than 1 K after adding CLW to the simulated BT. Moreover, the R^2 of each channel was above 0.95, indicating better matches between the observed and the simulated BTs with the addition of CLW information. Overall, the addition of CLW information could reduce the bias between the observed and the simulated BTs of MWR RPG during the no-precipitating cloud, and the correlation between the two was higher.
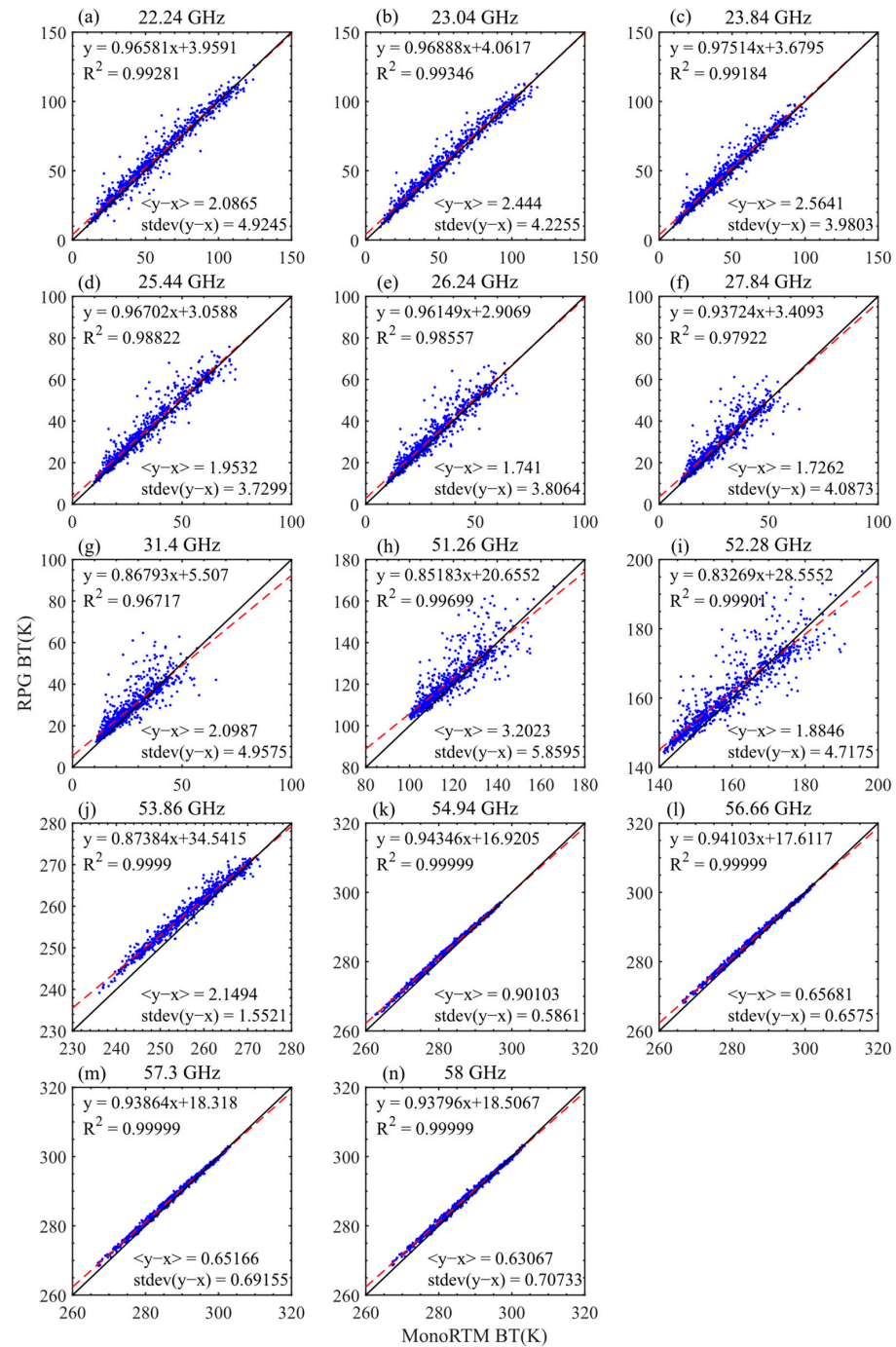
Figure 7. Scatter diagrams of observed BTs and simulated BTs (with CLW) in the no-precipitating cloudy weather (the red dashed lines are fitting straight lines). (**a**) 22.24 GHz, (**b**) 23.04 GHz, (**c**) 23.84 GHz, (**d**) 25.44 GHz, (**e**) 26.24 GHz, (**f**) 27.84 GHz, (**g**) 31.40 GHz, (**h**) 51.26 GHz, (**i**) 52.28 GHz, (**j**) 53.86 GHz, (**k**) 54.94 GHz, (**l**) 56.66 GHz, (**m**) 57.30 GHz, and (**n**) 58.00 GHz.

It should be noted that the outlier data points were removed using the pauta criterion in the scatter plot of no-precipitating cloudy weather conditions. It was found that the near-surface relative humidity of the sounding data at the time of removal was mostly above 90%, where fog might have occurred. This feature might provide some references for subsequent quality control before the application of MWR RPG products.

5. Accuracy of Temperature Retrieval Profiles and Performance of Temperature Inversion Retrieval

The performance of MWR RPG temperature profile retrieval products during various weather conditions was studied using sounding data. The pre-processed sample data were divided into three categories: clear-sky, no-precipitating cloud, and precipitating cloud, and their numbers were 302, 1038 and 189, respectively. The statistical analysis and the temperature inversion retrieval cases analysis were performed during various weather conditions.

5.1. Accuracy of Temperature Retrieval Profiles

Figure 8 shows the Bias and RMSE of temperature profiles with heights, respectively, for the clear-sky, no-precipitating cloud, and precipitating cloud. As can be seen from Figure 8, the trends of Bias and RMSE of the temperature profiles were consistent for the three weather conditions. Among them, the atmospheric temperature profiles retrieved by MWR RPG with precipitation had obvious positive biases at all heights, and RMSE values were all within 4 K. The biases of the other two atmospheric temperature profiles were around zero below 2 km height, and the RMSEs were below 2 K when the heights were below 4 km. In addition, the overall RMSE of the temperature profiles for all three weather conditions increased with height, so the retrieval accuracy of the MWR decreased with height. From the statistical analysis, the MWR had almost the same temperature profile retrieval accuracy during clear-sky and no-precipitating cloudy conditions, but the retrieval accuracy decreased significantly during precipitation. Therefore, the temperature profiles of MWR RPG retrieval, except for precipitation conditions, could be applied to the assimilation system with high reliability.
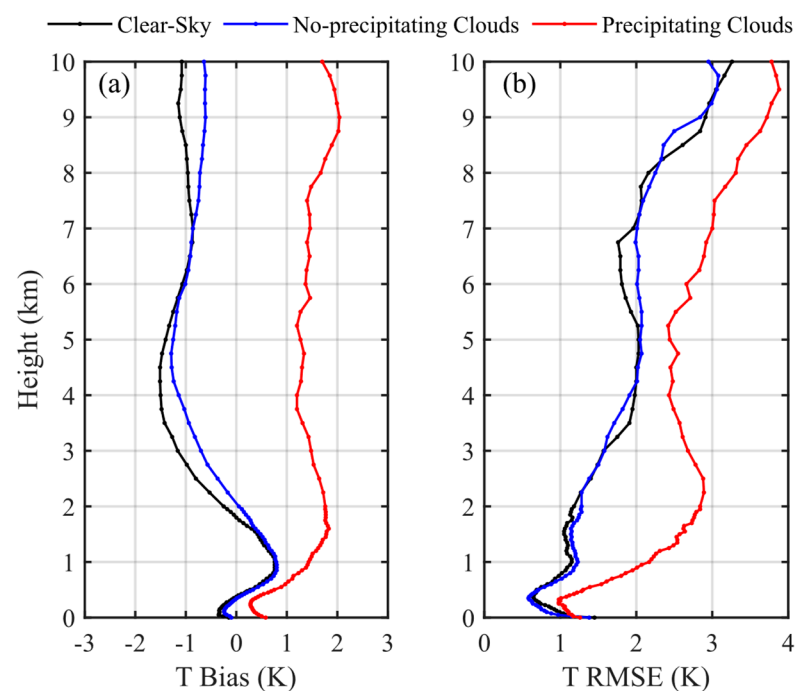

Figure 8. Variation diagrams of temperature profile Bias (**a**) and RMSE (**b**) with height for conditions of clear-sky (black), no-precipitating cloud (blue) and precipitating cloud (red).

5.2. Performance of the Temperature Inversion Retrieval

In the retrieval of temperature profiles, the temperature inversion characteristic is not easy to be retrieved. The study selected temperature profiles with temperature inversions during clear-sky and no-precipitating cloudy weather conditions to explore the performance of MWR RPG temperature retrievals. Figure 9 shows the comparison of the atmospheric temperature profiles of MWR RPG and RAOB for three cases of clear-sky conditions (Figure 9a–c) and no-precipitating cloudy conditions (Figure 9d–f). In Figure 9, the correlation coefficients (*r*) between the temperature profiles from the RPG retrieval and RAOB data were above 0.9, which indicated good agreements overall between these two profiles for these studied time periods. MWR RPG retrieval of the temperature inversions below 1 km (Figure 9a,e), had smoothed out amplitude and sharpness. When the atmospheric layer where the temperature inversion occurred was shallow (Figure 9b), or there was a double-layer temperature inversion (Figure 9d), the temperature inversions could not be well retrieved by MWR RPG. MWR RPG had limited retrieval ability for temperature inversion characteristics above 1 km, which even increased the error of retrieval of temperatures in the middle and upper troposphere (Figure 9c,f). Overall, MWR RPG had the potential ability to retrieve the temperature inversions in the boundary layer, which has important application value in fog and air pollution monitoring.
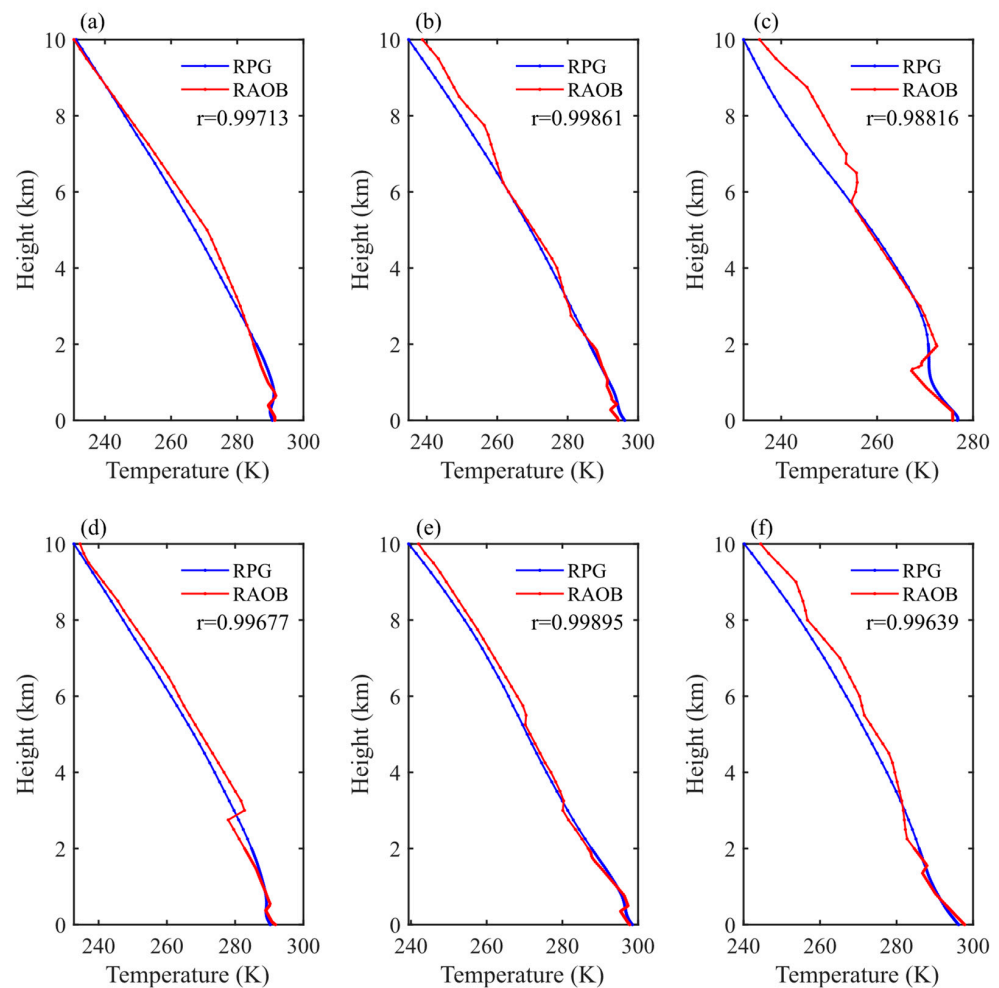

Figure 9. Temperature profiles in various weather conditions, where the blue line and the red line represent the MWR retrieval profiles (RPG) and the radiosonde observation profiles (RAOB), respectively. Temperature profiles observed at 1200 UTC on 17 April 2019 (**a**), 0000 UTC on 15 June 2019 (**b**), 0000 UTC on 27 December 2019 (**c**), 1200 UTC on 24 April 2019 (**d**), 0000 UTC on 16 June 2019 (**e**), and 1200 UTC on 18 September 2019 (**f**).

6. Conclusions

This study compared the 2017–2019 observations of RPG-HATPRO-G5 (the latest generation of ground-based multi-channel MWR installed in Shanghai, China) with the RAOB. The goal of this study was twofold. First of all, we compared the simulated BT of RAOB and the observed BT of MWR RPG during all-sky conditions, including precipitation times, followed by comparing them during non-precipitation conditions. In addition, when analyzing the observed BT performance during no-precipitating cloudy conditions, the impact of adding CLW information to BT simulation on evaluating BT performance was analyzed. Secondly, the accuracy of MWR RPG temperature profiles during various weather conditions was studied using RAOB data. For this purpose, this study carried out statistical analysis and temperature inversion retrieval cases analysis.

There was no significant change in the BT of each channel before and after the MWR calibration, so MWR RPG can operate stably. The detection performance of the near-surface temperature detection channels (56.66–58 GHz) was excellent compared with other channels, but the long-term time series analysis of these channels could reveal the seasonal variation bias characteristics. In addition, MWR RPG observed BTs were significantly higher during precipitation conditions. The simulated BTs and the observed BTs of MWR RPG matched well when clear-sky conditions were taken into account, but they did not match well in conditions of no-precipitating cloud. With the CLW added into the simulated BTs the discrepancies were reduced, as compared to RPG observed BTs, making both observed and simulated BTs more consistent. Specifically, by adding CLW information to the simulated BT, the bias and the SD of the observed BT and the simulated BT reduced and the R^2 value improved.

Regarding the retrieved temperature profiles from MWR RPG observed BT data, the statistical analysis showed that the performances for the clear-sky and no-precipitation conditions were better, as compared with RAOB, while the performance was worse for the case of precipitating cloudy conditions. The temperature profiles of the MWR RPG retrieval had the same accuracy of RMSEs with heights during both clear-sky and cloudy-sky conditions, where the RMSEs were below 2 K when the heights were below 4 km. The r between the temperature profiles from the MWR RPG retrievals and the RAOB profiles were above 0.9. Moreover, the MWR RPG can retrieve temperature inversions, which are below 1km, single layer and not shallow.

The ground-based MWR can provide BT observation data with high temporal resolution throughout the day as well as atmospheric profile retrieval products. Therefore, it plays an important role in monitoring the occurrence and development of important weather processes. This study can lay a certain foundation for the retrieval and the assimilation applications of ground-based MWR observations.

Institutional Review Board Statement: Not applicable.

Informed Consent Statement: Not applicable.

References

1. Wulfmeyer, V.; Hardesty, R.M.; Turner, D.D.; Behrendt, A.; Cadeddu, M.P.; Di Girolamo, P.; Schlüssel, P.; Van Baelen, J.; Zus, F. A Review of the Remote Sensing of Lower Tropospheric Thermodynamic Profiles and Its Indispensable Role for the Understanding and the Simulation of Water and Energy Cycles. *Rev. Geophys.* **2015**, *53*, 819–895. [CrossRef]
2. Cimini, D.; Haeffelin, M.; Kotthaus, S.; Löhnert, U.; Martinet, P.; O'Connor, E.; Walden, C.; Coen, M.C.; Preissler, J. Towards the Profiling of the Atmospheric Boundary Layer at European Scale—Introducing the COST Action PROBE. *Bull. Atmos. Sci. Technol.* **2020**, *1*, 23–42. [CrossRef]
3. Illingworth, A.J.; Cimini, D.; Gaffard, C.; Haeffelin, M.; Lehmann, V.; Löhnert, U.; O'Connor, E.J.; Ruffieux, D. Exploiting Existing Ground-Based Remote Sensing Networks to Improve High-Resolution Weather Forecasts. *Bull. Am. Meteorol. Soc.* **2015**, *96*, 2107–2125. [CrossRef]
4. Lei, L.; Lu, J.; Zhu, L.; Wu, H. Atmospheric Remote Sensing Using Multi-Channel Ground-Based Microwave Radiometer. *J. Remote Sens.* **2014**, *18*, 180–191. (In Chinese) [CrossRef]
5. De Angelis, F.; Cimini, D.; Löhnert, U.; Caumont, O.; Haefele, A.; Pospichal, B.; Martinet, P.; Navas-Guzmán, F.; Klein-Baltink, H.; Dupont, J.C.; et al. Long-Term Observations Minus Background Monitoring of Ground-Based Brightness Temperatures from a Microwave Radiometer Network. *Atmos. Meas. Tech.* **2017**, *10*, 3947–3961. [CrossRef]
6. Liu, H. The Temperature Profile Comparison between the Ground-Based Microwave Radiometer and the Other Instrument for the Recent Three Years. *Acta Meteorol. Sin.* **2011**, *69*, 719–728. (In Chinese) [CrossRef]
7. Ahn, M.H.; Won, H.Y.; Han, D.; Kim, Y.H.; Ha, J.C. Characterization of Downwelling Radiance Measured from a Ground-Based Microwave Radiometer Using Numerical Weather Prediction Model Data. *Atmos. Meas. Tech.* **2016**, *9*, 281–293. [CrossRef]
8. Clough, S.A.; Shephard, M.W.; Mlawer, E.J.; Delamere, J.S.; Iacono, M.J.; Cady-Pereira, K.; Boukabara, S.; Brown, P.D. Atmospheric Radiative Transfer Modeling: A Summary of the AER Codes. *J. Quant. Spectrosc. Radiat. Transf.* **2005**, *91*, 233–244. [CrossRef]
9. Hewison, T.J.; Gaffard, C. 1D-VAR Retrieval of Temperature and Humidity Profiles from Ground-Based Microwave Radiometers. In Proceedings of the 2006 IEEE MicroRad, 9th Specialist Meeting on Microwave Radiometry and Remote Sensing Applications, MicroRad'06, San Juan, PR, USA, 28 February–3 March 2006; IEEE: Piscataway, NJ, USA, 2006; pp. 235–240. [CrossRef]
10. Güldner, J.; Spänkuch, D. Remote Sensing of the Thermodynamic State of the Atmospheric Boundary Layer by Ground-Based Microwave Radiometry. *J. Atmos. Ocean. Technol.* **2001**, *18*, 925–933. [CrossRef]
11. Solheim, F.; Godwin, J.R.; Westwater, E.R.; Han, Y.; Keihm, S.J.; Marsh, K.; Ware, R. Radiometric Profiling of Temperature, Water Vapor and Cloud Liquid Water Using Various Inversion Methods. *Radio Sci.* **1998**, *33*, 393–404. [CrossRef]
12. Li, Q.; Wei, M.; Wang, Z.; Chu, Y. Evaluation and Improvement of the Quality of Ground-Based Microwave Radiometer Clear-Sky Data. *Atmosphere* **2021**, *12*, 435. [CrossRef]
13. Li, Q.; Wei, M.; Wang, Z.; Jiang, S.; Chu, Y. Improving the Retrieval of Cloudy Atmospheric Profiles from Brightness Temperatures Observed with a Ground-Based Microwave Radiometer. *Atmosphere* **2021**, *12*, 648. [CrossRef]
14. Tan, H.; Mao, J.; Chen, H.; Chan, P.W.; Wu, D.; Li, F.; Deng, T. A Study of a Retrieval Method for Temperature and Humidity Profiles from Microwave Radiometer Observations Based on Principal Component Analysis and Stepwise Regression. *J. Atmos. Ocean. Technol.* **2011**, *28*, 378–389. [CrossRef]
15. Chan, P.W. Performance and Application of a Multi-Wavelength, Ground-Based Microwave Radiometer in Intense Convective Weather. *Meteorol. Z.* **2009**, *18*, 253–265. [CrossRef]
16. Xu, G.; Xi, B.; Zhang, W.; Cui, C.; Dong, X.; Liu, Y.; Yan, G. Comparison of Atmospheric Profiles between Microwave Radiometer Retrievals and Radiosonde Soundings. *J. Geophys. Res. Atmos.* **2015**, *120*, 10313–10323. [CrossRef]
17. Bedoya-Velásquez, A.E.; Navas-Guzmán, F.; de Arruda Moreira, G.; Román, R.; Cazorla, A.; Ortiz-Amezcua, P.; Benavent-Oltra, J.A.; Alados-Arboledas, L.; Olmo-Reyes, F.J.; Foyo-Moreno, I.; et al. Seasonal Analysis of the Atmosphere during Five Years by Using Microwave Radiometry over a Mid-Latitude Site. *Atmos. Res.* **2019**, *218*, 78–89. [CrossRef]
18. Ware, R.; Carpenter, R.; Güldner, J.; Liljegren, J.; Nehrkorn, T.; Solheim, F.; Vandenberghe, F. A Multichannel Radiometric Profiler of Temperature, Humidity, and Cloud Liquid. *Radio Sci.* **2003**, *38*, 8079. [CrossRef]
19. Caumont, O.; Cimini, D.; Löhnert, U.; Alados-Arboledas, L.; Bleisch, R.; Buffa, F.; Ferrario, M.E.; Haefele, A.; Huet, T.; Madonna, F.; et al. Assimilation of Humidity and Temperature Observations Retrieved from Ground-Based Microwave Radiometers into a Convective-Scale NWP Model. *Q. J. R. Meteorol. Soc.* **2016**, *142*, 2692–2704. [CrossRef]
20. He, W.; Chen, H.; Li, J. Influence of Assimilating Ground-Based Microwave Radiometer Data into the WRF Model on Precipitation. *Atmos. Ocean. Sci. Lett.* **2020**, *13*, 107–112. [CrossRef]

21. Qi, Y.; Fan, S.; Mao, J.; Li, B.; Guo, C.; Zhang, S. Impact of Assimilating Ground-Based Microwave Radiometer Data on the Precipitation Bifurcation Forecast: A Case Study in Beijing. *Atmosphere* **2021**, *12*, 551. [CrossRef]
22. Qi, Y.; Fan, S.; Li, B.; Mao, J.; Lin, D. Assimilation of Ground-Based Microwave Radiometer on Heavy Rainfall Forecast in Beijing. *Atmosphere* **2022**, *13*, 74. [CrossRef]
23. Temimi, M.; Fonseca, R.M.; Nelli, N.R.; Valappil, V.K.; Weston, M.J.; Thota, M.S.; Wehbe, Y.; Yousef, L. On the Analysis of Ground-Based Microwave Radiometer Data during Fog Conditions. *Atmos. Res.* **2020**, *231*, 104652. [CrossRef]
24. Turner, D.D.; Kneifel, S.; Cadeddu, M.P. An Improved Liquid Water Absorption Model at Microwave Frequencies for Supercooled Liquid Water Clouds. *J. Atmos. Ocean. Technol.* **2016**, *33*, 33–44. [CrossRef]